Microstructural and micromagnetic characterization of thin film magnetic tunnel junctions

R. E. Dunin-Borkowski,[a] M. R. McCartney, and David J. Smith[b]
Center for Solid State Science, Arizona State University, Tempe, Arizona 85287-1704

S. Gider, B.-U. Runge, and S. S. P. Parkin
IBM Almaden Research Center, 650 Harry Road, San Jose, California 95120-6099

High-resolution electron microscopy, Lorentz microscopy, and off-axis electron holography have been used to characterize magnetic tunnel junctions. Observations in cross section show that the tunnel barriers are slightly narrower and smoother after annealing at temperatures up to 350 °C. The demagnetization of a magnetically hard CoPtCr reference layer through repeated magnetization reversal of a soft layer of either Co or $Ni_{40}Fe_{60}$ is likely to originate from magnetic fringing fields at Néel walls, which form in the soft layers close to the coercive field. © *1999 American Institute of Physics.* [S0021-8979(99)61308-1]

I. INTRODUCTION

Magnetic tunnel junctions (MTJs) have attracted increased interest in recent years.[1–3] These junctions usually contain ferromagnet–insulator–ferromagnet combinations, and their use is based on the large (magneto-) resistance changes that occur during magnetization reversal.[1] Transmission electron microscopy (TEM) is one of the most powerful techniques available for providing microstructural and micromagnetic information at resolution levels that can be approached by few other analytical techniques. In this article, we have used combinations of high-resolution electron microscopy, Lorentz microscopy, and off-axis electron holography to characterize thin film tunnel junctions. These MTJs contain CoPtCr (''hard'') ferromagnetic layers, alumina insulating barriers, and CoPt, Co, or NiFe (''soft'') ferromagnetic layers. We begin with an assessment of the effect of annealing on the integrity of the alumina tunnel barrier. We then address the mechanism of magnetization decay of the hard layer following repeated reversal of the soft layers.

II. EXPERIMENTAL DETAILS

The samples described here were prepared using magnetron sputter deposition at room temperature, either onto thermally oxidized Si substrates (for cross-sectional observations) or onto electron-transparent silicon nitride membranes or holey carbon films (for plan-view observations). High-resolution studies utilized a JEM-4000EX TEM operated at 400 keV, while micromagnetic observations were performed at 200 keV on a Philips CM-200 field emission gun TEM equipped with an auxiliary (Lorentz) minilens and an electrostatic biprism in the selected area aperture plane. Samples could then be examined in close to field-free conditions with the conventional microscope objective lens switched off. Alternatively, the objective lens could be excited slightly and the sample tilted in order to apply a known in-plane field so that magnetization reversal processes could be observed *in situ*.

III. RESULTS AND DISCUSSION

A. Cross-sectional geometry

The effect of moderate annealing on the width and roughness of the tunnel barrier is an important issue for the integration of MTJs with Si processing technology, for example for magnetic memory applications. MTJs consisting of, nominally, Si(001)|500 nm SiO_2|25 nm $Cr_{0.8}V_{0.2}$|15 nm $Co_{0.75}Pt_{0.12}Cr_{0.13}$|1.4 nm Al plasma oxidized for 240 s|15 nm $Co_{0.88}Pt_{0.12}$|20 nm Al were annealed for 30 min at temperatures of 250, 300, and 350 °C. High-resolution observations confirmed the crystallinity of the ferromagnetic layers and showed that the continuity of the barrier was maintained after annealing. Figure 1 shows a representative cross-sectional image of a CoPtCr/AlO_x/CoPt tunnel junction, as deposited. From images such as these, both the amorphous nature and the integrity of the tunnel barrier were confirmed for all annealing temperatures. Local changes in the width of the barriers and longer-range waviness were observed. Measure-

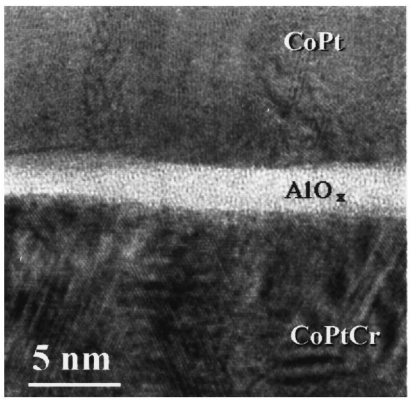

FIG. 1. Representative cross-sectional image of CoPtCr/AlO_x/CoPt tunnel junction, as deposited.

[a]Current address: Department of Materials, Parks Road, Oxford 0X1 3PH, UK; electronic mail: rafal.db@materials.oxford.ac.uk
[b]Also with: Department of Physics and Astronomy, Arizona State University.

 © 1999 American Institute of Physics

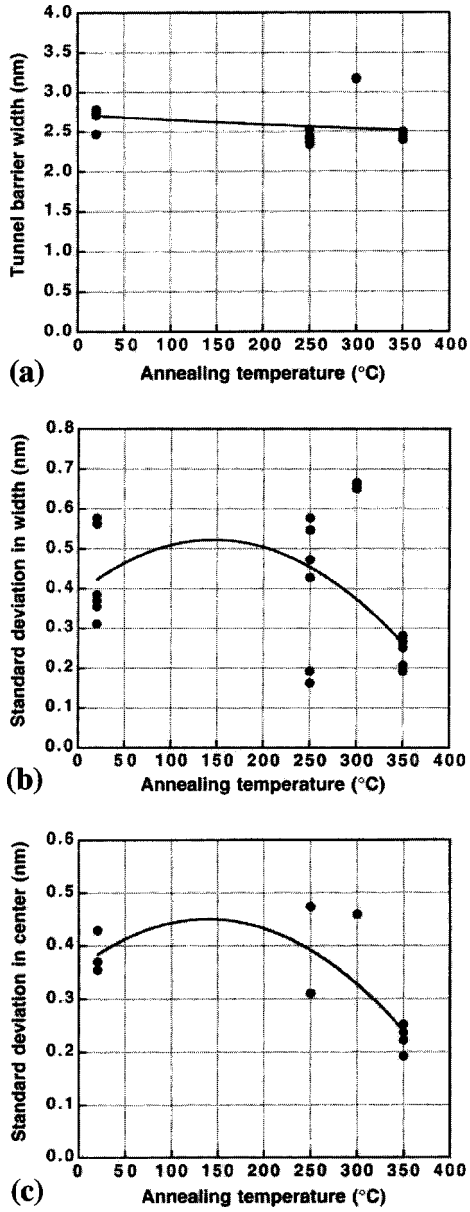

FIG. 2. Characteristics of alumina tunnel barrier as function of annealing temperature as measured from high-resolution images: (a) tunnel barrier width; (b) the standard deviation in this mean width; and (c) the standard deviation in the position of the center of the layer.

ments of the mean barrier width, the standard deviation in this mean width, and the standard deviation in the position of the center of the layer are shown in Fig. 2, both for different regions from a single sample and for samples obtained from different regions of a wafer. The data were always acquired from areas that were thin enough to show lattice fringes, so that variations along the beam direction are less likely. Least-squares (quadratic) fits to the data are also shown for illustrative purposes only. Although there are considerable variations from area to area even for the same annealing temperature, Fig. 2 shows that the mean layer width is on average 10% smaller after annealing at 350 °C than after deposition at room temperature. Both the local variation in the layer width and the longer-range roughness are also slightly smaller after annealing. It should be noted that considerable care was taken to ensure that the results were not affected by the procedures used to prepare the cross-sectional samples, and in particular by ion-beam thinning.

B. Plan-view geometry

The use of MTJs as potential magnetic memory storage cells relies on devising MTJs with two stable magnetic states (the magnetic moments of the two ferromagnetic layers being parallel or antiparallel).[4] Repeated reversal of the magnetization of soft ferromagnetic layers of either Co or $Ni_{40}Fe_{60}$ has recently been observed to cause demagnetization of a second, magnetically hard reference layer of $Co_{0.75}Pt_{0.12}Cr_{0.13}$. This process is thought to be caused by the motion of domain walls during magnetization reversal, and would erase the tunnel junction's memory.[4] The rate of decay was much faster for a Co soft layer than for NiFe. Lorentz microscopy and electron holography were used to investigate the mechanisms of magnetization reversal and hard layer decay in these structures, which comprised 15 nm Cr|10 nm $Co_{0.75}Pt_{0.12}Cr_{0.13}$|1.2 nm Al plasma oxidized for 240 s |15 nm Co or $Ni_{40}Fe_{60}$|5 nm Cr.

Lorentz microscopy (out-of-focus, or Fresnel imaging)[5] was used to study the formation and movement of domain walls during magnetization reversal of each soft layer, with the hard layer fully magnetized. The magnetization direction of each soft layer rotated slightly as its coercive field was approached, together with a marked strengthening of the magnetization ripple. At the coercive field, large sections of the soft layer reversed in succession, while other regions remained pinned to slightly higher applied fields, possibly by features associated with the underlying hard layer. Figure 3 shows Lorentz images of the Co [Fig. 3(a)] and the NiFe [Fig. 3(b)] soft layers, taken at the coercive field under identical defocus and illumination conditions, with the underlying hard layer fully magnetized in the direction of the arrow. In each image, some of the soft layer has reversed (these regions correspond to the smoother contrast), while other regions are about to reverse (these correspond to the stronger contrast). The strong black/white lines are domain walls, and their contrast is strongest at the edges of the regions where the magnetization direction has already reversed. The contrast of the walls is stronger in Co than in NiFe, although the mechanism of magnetization reversal appears to be very similar for the two films.

Off-axis electron holography allows both the magnitude and the direction of the local magnetization at domain walls to be quantified.[6] A positive voltage is applied to an electrostatic biprism wire to overlap an electron wave that has passed through the sample with one that has passed only through vacuum. The amplitude and the phase of the electron wave are recorded in the intensity and the position of the resulting interference fringes, respectively. The phase is sensitive to the in-plane component of the magnetic induction integrated in the incident beam direction.[7] Additional reference holograms are recorded in the absence of the sample in order to exclude artifacts associated with the imaging and recording systems.[8] Further details of the practical requirements for off-axis electron holography, including informa-

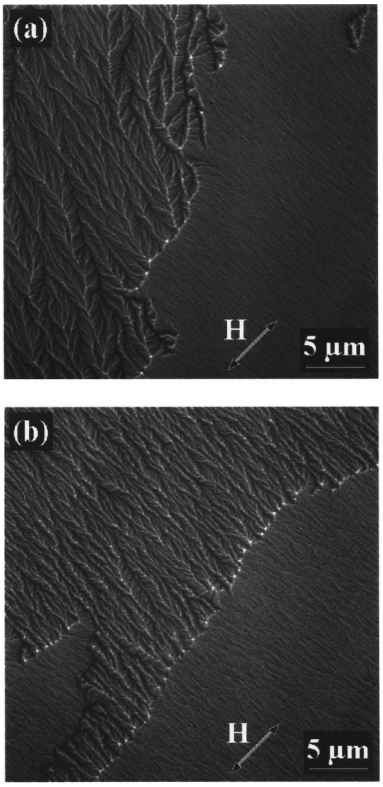

FIG. 3. Lorentz images at coercive field during magnetization reversal of: (a) 15 nm Co soft layer and (b) 15 nm $Ni_{40}Fe_{60}$ soft layer, with underlying 10 nm CoPtCr layer fully magnetized in the direction of the arrow.

tion about recording and processing holograms, can be found elsewhere.[9]

Figure 4 shows results obtained using Lorentz microscopy and off-axis electron holography to study domain walls in the two soft layers alone (i.e., without the hard layers present). These layers were deposited onto holey carbon films specifically so that a vacuum wave could be overlapped onto the sample at the edge of a hole. Figure 4(a) shows Lorentz images of the areas that were used for holography, while Fig. 4(b) shows phase contour lines overlaid onto the electron holographic phase images extracted from the areas outlined in Fig. 4(a). (The black areas were outside the holographic interference region, and have been scaled to zero in the images as they contained no phase information.) The contours in Fig. 4(b) lie parallel to lines of constant magnetic induction: they would be exactly parallel to the in-plane magnetization in the absence of demagnetizing fields. Prominent domain walls and vortices are visible where the direction of the contours changes in each image. The *magnitude* of the in-plane magnetic induction integrated in the incident beam direction is shown for each sample in Fig. 4(c). The intensity of some of the domain walls is closely similar to that of the surrounding domains in Fig. 4(c). One such wall is marked A in the figure. These are Neel walls, at which the magnetization reverses in the plane of the foil. However, some of the walls (such as the wall marked B in the figure) appear dark, indicating that the in-plane component of the magnetization integrated in the incident beam direction is reduced from that in the domains. Although the darker contrast could be explained by the presence of asymmetric Bloch walls,[10] which contain a magnetic vortex with an axis in the plane of the film, it is unlikely that these can form in a Co or NiFe film that has a thickness of only 15 nm.[11] The dark contrast may instead be associated with the presence of asymmetric Néel walls,[12] which have an out-of-plane component of the field within the film thickness. Moreover, the magnetic properties of Co and NiFe suggest that strong magnetic fringing fields should originate from both types of Néel wall and that they should be stronger for Co than for NiFe.[11] Thus, it is likely that the decay of the hard layer is associated with interactions between the two ferromagnetic films at the positions of the Néel walls in the soft layers. Further details about the magnetic microstructure and the mechanisms of magnetization reversal in these tunnel junctions will be described elsewhere.

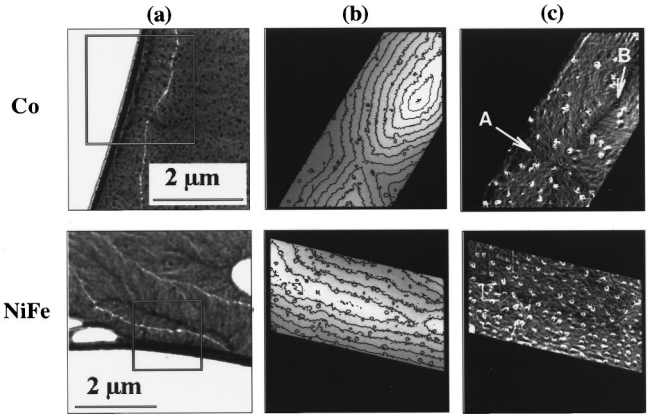

FIG. 4. (a) Lorentz images of domain walls in soft layers alone supported on holey carbon film. (b) Contours superimposed on electron holographic phase image of areas marked in (a). (c) Magnitude of in-plane component of magnetic induction integrated in incident beam direction. Features of interest are dark lines at positions of domain walls, which provide evidence for presence of asymmetric Néel walls. (Small white circles are surface oxide particles; their contrast is not magnetic.)

ACKNOWLEDGMENTS

The authors thank J. Miltat and M. R. Scheinfein for discussions and James Speidell at IBM for providing silicon nitride membranes. This work was supported by an IBM subcontract on the DARPA Advanced MRAM project under Contract No. MDA-972-96-C-0014.

[1] W. J. Gallagher, S. S. P. Parkin, Y. Lu, X. P. Bian, A. Marley, K. P. Roche, R. A. Altman, S. A. Rishton, C. Jahnes, T. M. Shaw, and G. Xiao, J. Appl Phys. **81**, 3741 (1997).
[2] J. S. Moodera, L. R. Kinder, T. M. Wong, and R. Meservey, Phys. Rev. Lett. **74**, 3273 (1995).
[3] J. S. Moodera and L. R. Kinder, J. Appl. Phys. **79**, 4724 (1996).
[4] S. Gider, B.-U. Runge, A. C. Marley, and S. S. P. Parkin, Science **281**, 797 (1998).
[5] J. N. Chapman, J. Phys. D **17**, 623 (1984).
[6] M. R. McCartney and Y. Zhu, Appl. Phys. Lett. **72**, 1380 (1998).
[7] A. Tonomura, Adv. Phys. **41**, 59 (1992).
[8] W. J. de Ruijter and J. K. Weiss, Ultramicroscopy **50**, 269 (1993).
[9] D. J. Smith and M. R. McCartney, in *Introduction to Electron Holography*, edited by E. Völkl, L. F. Allard, and D. C. Joy (Plenum, New York, 1999), Chap. 4.
[10] A. E. LaBonte, J. Appl. Phys. **420**, 2450 (1969).
[11] M. R. Scheinfein, Department of Physics and Astronomy, Arizona State University (private communication, 1998).
[12] A. Hubert, Phys. Status Solidi **38**, 699 (1970).